Synchrotron powder diffraction, X-ray absorption and ^{1}H nuclear magnetic resonance data for hypoxanthine, $C_5H_4N_4O$

Joel Reid,[1,a)] Toby Bond,[1] Shiliang Wang,[2] Jigang Zhou,[1] and Anguang Hu[2]
[1]*Canadian Light Source, 44 Innovation Boulevard, Saskatoon, SK, Canada S7N 2V3*
[2]*Defence Research & Development Canada Suffield, Medicine Hat, AB, Canada T1A 8K6*

(Received 23 January 2015; accepted 30 April 2015)

Synchrotron powder X-ray diffraction, X-ray absorption spectroscopy (XAS), and proton nuclear magnetic resonance (^{1}H-NMR) data have been used to examine the structure of hypoxanthine, 1,7-dihydro-6H-purin-6-one ($C_5H_4N_4O$), a purine base that participates in numerous metabolic processes. XAS and ^{1}H-NMR spectroscopy were used to determine that hypoxanthine was present in its keto form (both in solid state and dissolved in an organic solvent). Rigid body refinement was performed with the Rietveld software package GSAS yielding triclinic lattice parameters of $a = 7.1179$ (2) Å, $b = 9.7830$ (3) Å, $c = 10.4009$ (3) Å, $\alpha = 58.876$ (1)°, $\beta = 67.609$ (1)°, and $\gamma = 71.937$ (2)° ($C_5H_4N_4O$, $Z = 4$, space group $P\bar{1}$). © *2015 International Centre for Diffraction Data.*
[doi:10.1017/S0885715615000457]

Key words: hypoxanthine, synchrotron, powder diffraction, X-ray absorption spectroscopy, nuclear magnetic resonance

I. INTRODUCTION

Hypoxanthine is a natural purine derivative and deamination product of adenine [$C_5H_5N_5$, one of the two purine bases found in deoxyribonucleic acid (DNA), and ribonucleic acid (RNA)], forming as an intermediate product prior to uric acid ($C_5H_4N_4O_3$) during metabolic breakdown (Sarkar and Nahar, 2007). Defects in purine metabolism can result in significant uptake of hypoxanthine in DNA and RNA, which may impede RNA function and gene expression (Pang *et al.*, 2012), and hypoxanthine has been observed as a constituent in riboswitches, which acts as control mechanisms for cellular metabolism (Batey *et al.*, 2004). The levels of purine metabolites are highly regulated in the body and hypoxanthine imbalances may be linked with numerous issues from the formation of crystalline hypoxanthine in muscle tissue (Parker *et al.*, 1969) to the occurrence of gout (Puig *et al.*, 1988).

The structure of hypoxanthine was originally determined by Schmalle *et al.* (1988) using single-crystal X-ray diffraction (XRD). Figure 1 shows the structure, corresponding to the keto N9H tautomer, illustrating two crystallographically independent molecules (molecules *A* and *B*) in the triclinic unit cell. Currently, a single low-precision, unindexed, experimental powder diffraction pattern appears for hypoxanthine in the Powder Diffraction File (ICDD, 2013) (PDF 00-007-0712), although an additional pattern (PDF 02-064-3532) calculated from the crystal structure of Schmalle *et al.* (1988) is included in the PDF-4 Organics database. A second calculated entry in the PDF-4 Organics database, based on a recent single-crystal study by Yang and Xie (2007), suggests the existence of an additional monoclinic polymorph of hypoxanthine. This paper examines the Rietveld refinement of hypoxanthine using rigid body refinement with the Rietveld package GSAS/EXPGUI, and provides a complete reflection list for phase identification, as well as a comparison of experimental proton nuclear magnetic resonance (^{1}H-NMR) data with theoretical density functional theory calculations.

II. EXPERIMENTAL

Adenine (≥99%) was purchased from Sigma-Aldrich (Sigma A8626) and used without further purification. Hypoxanthine was produced by slow spontaneous deamination of adenine in an aqueous solution under ambient conditions. After 10 weeks of slow reaction, adenine was fully converted to hypoxanthine. Hypoxanthine was crystallized by slow evaporation from aqueous solution at 80 °C on a hot plate. No detectable by-products were observed by Raman spectroscopy.

X-ray absorption near edge structure (XANES) spectra were collected using the Spherical Grating Monochromator beamline (SGM or 11ID-1) at the Canadian Light Source (CLS). 11ID-1 employs a 45 mm planar undulator source with a spherical grating Dragon-type monochromator using three gratings to cover the energy range between 250 and 2000 eV. The nominal beam size on the sample was 100 × 1000 μm^2. An aqueous solution of hypoxanthine was drop coated onto a gold-coated silicon wafer, and then air dried prior to data collection. Two to four spectra were collected in partial fluorescence yield step scanning at the carbon and oxygen *K*-edges using a step size of 0.1 eV and a 1 s dwell time. The spectra were normalized by dividing by the incident flux (I_0), which was obtained by measuring the total electron yield from a gold mesh. The photon energy was calibrated using graphite for the C *K*-edge (285.5 eV, Zhou *et al.*, 2014) and using Li_2O_2 for the O *K*-edge (532.3 eV, Gallant *et al.*, 2012).

^{1}H-NMR data were collected at the Saskatchewan Structural Sciences Center (SSSC) using a Bruker Advance

a)Author to whom correspondence should be addressed. Electronic mails: joel.reid@lightsource.ca, joelwreid@gmail.com

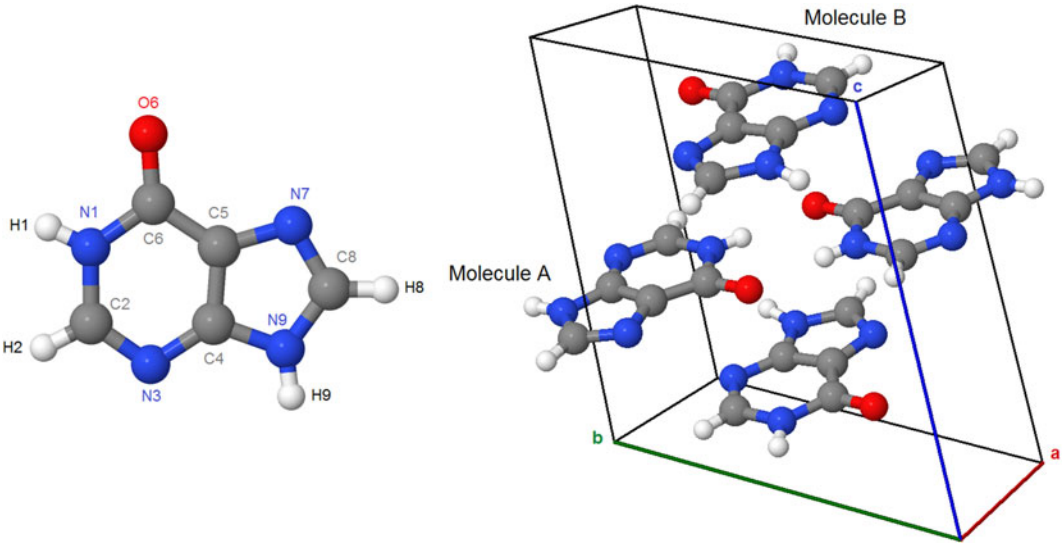

Figure 1. (color online) An illustration of the atomic labeling of hypoxanthine (N9H tautomer, left) and the triclinic unit cell of hypoxanthine, with both independent molecules labeled (right).

500 MHz NMR spectrometer. The spectrum was acquired using 256 scans so as to maximize the signal-to-noise ratio for accurate integration of broadened amine and/or hydroxyl peaks. Six mg of hypoxanthine powder was transferred into a NMR tube using a spatula, and the sample was dissolved in approximately 1 ml of deuterated dimethyl sulfoxide (DMSO). To completely dissolve the sample in DMSO, the tube was sonicated in an ultrasonic water bath at room temperature for approximately 30 min until no undissolved powder was visible. The spectrum was processed and analyzed using the Spinworks 4.0 software package (Marat, 2014).

Powder X-ray diffraction (PXRD) patterns were collected using a Canadian Macromolecular Crystallography Facility beamline (CMCF-BM or 08B1-1) at the CLS. 08B1-1 is a bending magnet beamline where the photon energy is selected with a Si (111) double-crystal monochromator. The hypoxanthine powder was loaded, with no grinding, into a 0.5 mm ID Kapton capillary which was sealed at both ends with a Loctite adhesive. Two-dimensional (2D) PXRD patterns were obtained using a Rayonix MX300HE detector with an active area of 300×300 mm^2. The patterns were collected at an energy of 18 keV ($\lambda = 0.688\,80$ Å) and capillary–detector distance of 250 mm.

The 2D PXRD patterns were calibrated and integrated using the GSASII software package (Toby and Von Dreele, 2013). The sample–detector distance, detector centering, and tilt were calibrated using a lanthanum hexaboride (LaB_6) standard reference material (NIST SRM 660a LaB_6) and the calibration parameters were applied to all patterns. After calibration, the 2D patterns were integrated to obtain the standard PXRD patterns. A pattern from an empty 0.5 mm ID Kapton capillary (collected using the same conditions) was subtracted from the sample data during integration. The integrated LaB_6 pattern was used to obtain the instrument resolution of the beamline for the refinement of the hypoxanthine sample.

The single-crystal structure of Schmalle *et al.* (1988) was used as an initial model for the refinement. Rigid body Rietveld refinement was performed with the GSAS/EXPGUI program (Toby, 2001; Larson and Von Dreele, 2004). The implementation of rigid body refinements in GSAS and EXPGUI has been described previously in the literature (Dinnebier, 1999; Lake and Toby, 2011). Rigid bodies were created for both independent hypoxanthine molecules, including the hydrogen atoms. The carbon, nitrogen, and oxygen atoms were refined with an overall isotropic displacement parameter (U_{iso}), whereas the hydrogen atoms were constrained to a U_{iso} value of 1.3 times the heavier atoms. Toward the end of the refinement, the positions of the hydrogen atoms were optimized with the Mercury 3.3 module of the Cambridge Structural Database (Allen, 2002). The background was refined using an orthogonal Chebyschev polynomial. The crystal data, data collection, and refinement details are summarized in Table I.

TABLE I. The crystal data, data collection, and refinement parameters obtained for the hypoxanthine refinement.

Crystal data	
Formula, Z	$C_5H_4N_4O$, $Z = 4$
Molecular mass (M_r)	136.11 g mol^{-1}
Symmetry, space group	Triclinic, $P\bar{1}$
Unit-cell parameters	$a = 7.1179$ (2) Å, $b = 9.7830$ (3) Å, $c = 10.4009$ (3) Å, $\alpha = 58.876$ (1)°, $\beta = 67.609$ (1)°, $\gamma = 71.937$ (2)°
Volume	567.37 (2) Å^3
Data collection	
Beamline	Canadian Light Source (CLS) 08B1-1
Specimen mounting	0.5 mm ID Kapton capillary
Collection mode	Transmission
Energy, wavelength	18 keV, $\lambda = 0.688\,80$ Å
Collection range, step size	2°–37° (2θ), 0.005° step^{-1}
Temperature	293 K
Refinement	
Number of data points	6999
Number of refined parameters	51
R_p	0.0624
R_{wp}	0.0831
R_{exp}	0.0726
χ^2	1.32

https://doi.org/10.1017/S0885715615000457 Published online by Cambridge University Press

Ab initio calculation of the ^{1}H isotropic magnetic shielding was carried out at the B3LYP/6-311+G(d,p) theory level (Becke, 1988; Lee *et al.*, 1988) using Q-Chem 4.1 (Krylov and Gill, 2013). The chemical shifts were converted from the isotropic magnetic shielding:

$$\delta_H = \delta_{\text{isotropic (DMSO)}} - \delta_{H\text{ (calculated isotropic magnetic shielding)}}$$

where $\delta_{\text{isotrophic(DMSO)}}$ is 32. No hydrogen bonding or anisotropic effects were taken into account in the calculations.

III. RESULTS AND DISCUSSION

Hypoxanthine can exist in either its keto or enol tautomer. Figure 2 shows the structure of both of these tautomers for hypoxanthine, differentiated by protons H_1 and H_6. In addition, two keto tautomers have been observed with protons on either the N_7 (N7H tautomer) or N_9 (N9H tautomer) sites. To verify which tautomer of hypoxanthine was present in the sample, C and O *K*-edge XANES and ^{1}H-NMR spectra were obtained.

Figures 3(a) and 3(b) illustrate the XANES spectra for the C and O *K*-edges, respectively. The prominent peaks at 287.8 eV in the C *K*-edge and 532.2 eV in the O *K*-edge have been studied previously in purines (Samuel *et al.*, 2006; Zubavichus *et al.*, 2008) and assigned to π^* carbonyl (C=O) bonding, suggesting that the keto tautomer of hypoxanthine is present in the solid.

The single-crystal XRD study of Schmalle *et al.* (1988) concluded that both crystallographically independent hypoxanthine molecules *A* and *B* were predominantly the N9H tautomer in the solid state, but could not definitively exclude the minor presence of other tautomers based on the final difference Fourier synthesis. In the work presented here, the N9H starting model was used for the PXRD refinement, but tests were also performed by adding the H_7 proton in ideal positions for both molecules, and constraining the H_7 and H_9 occupancies to be equal to 1 (starting with an equal fraction between them). Although the results were sensitive to the stage of refinement and starting conditions, the H_7 occupancy always yielded a negative value for molecule *B* (with a corresponding H_9 occupancy greater than 1), and generally yielded either a negative or quite small value for molecule *A*. Given the low atomic scattering factor for hydrogen with X-rays, this result is not definitive, but the final refinement was conducted assuming both molecules are present as the N9H tautomer. Figure 4 illustrates the final Rietveld refinement of

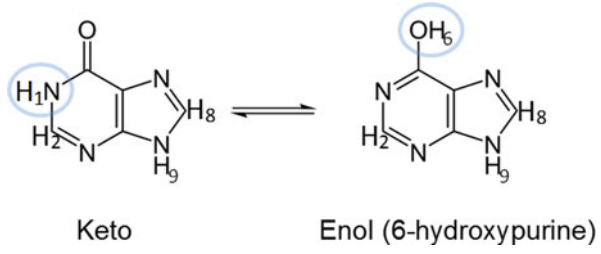

Figure 2. (color online) Structures of the keto and enol N9H tautomers of hypoxanthine. The highlighted protons give rise to expected differences in their respective ^{1}H-NMR spectra.

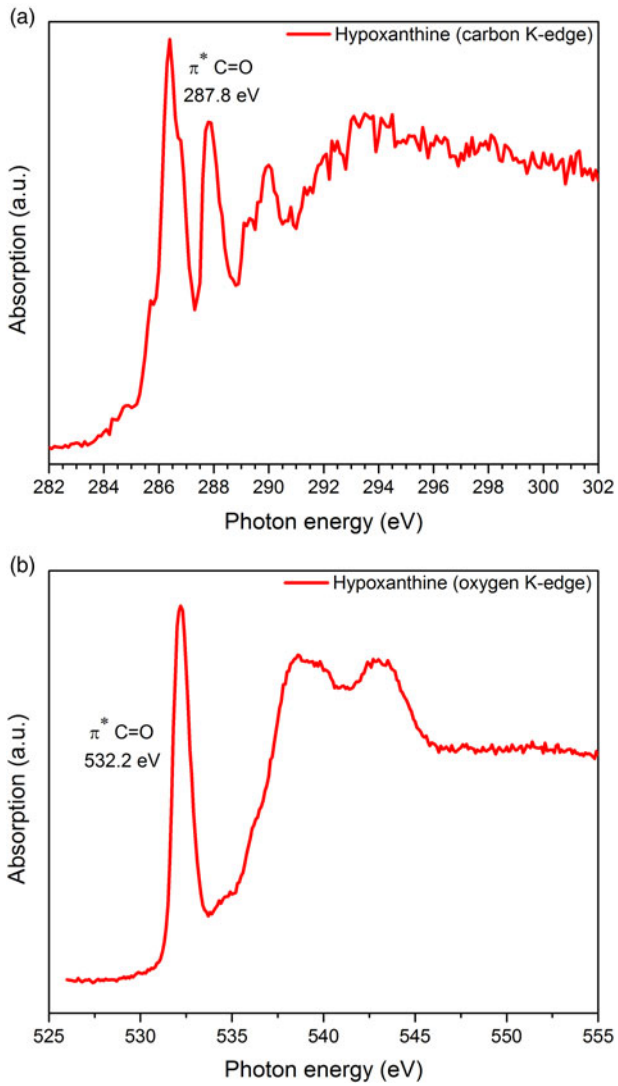

Figure 3. (color online) The carbon (a) and oxygen (b) *K*-edge XANES spectra obtained for hypoxanthine. The strong peak at 286.5 eV is because of π^* C–N bonding (Samuel *et al.*, 2006).

hypoxanthine obtained with GSAS, whereas the refined atomic coordinates are shown in Table II. Similar to previous 2D data obtained for curcumin (Reid *et al.*, 2015), hypoxanthine exhibited graininess but even mild grinding resulted in significant reflection broadening, making the 2D detector crucial for obtaining reasonable intensity estimates.

A comparison of hydrogen-bonding distances from the PXRD and single-crystal refinement of Schmalle *et al.* (1988) are given in Table III. The single-crystal and powder results are quite consistent, with only slight discrepancies observed in the bond lengths greater than 3 Å.

A reflection list for hypoxanthine was prepared by summing adjacent reflections with relative integrated intensities larger than 0.1% and closer than 0.02° 2θ as multiple reflections and assigning a weighted average reflection position. The final reflection list in Table IV contains all reflections with relative integrated intensities greater than or equal to 0.3%.

The ^{1}H-NMR spectrum of hypoxanthine in solution was acquired at room temperature using deuterated DMSO as the solvent. Figures 5(a) and 5(b) show the ^{1}H-NMR spectrum

https://doi.org/10.1017/S0885715615000457 Published online by Cambridge University Press

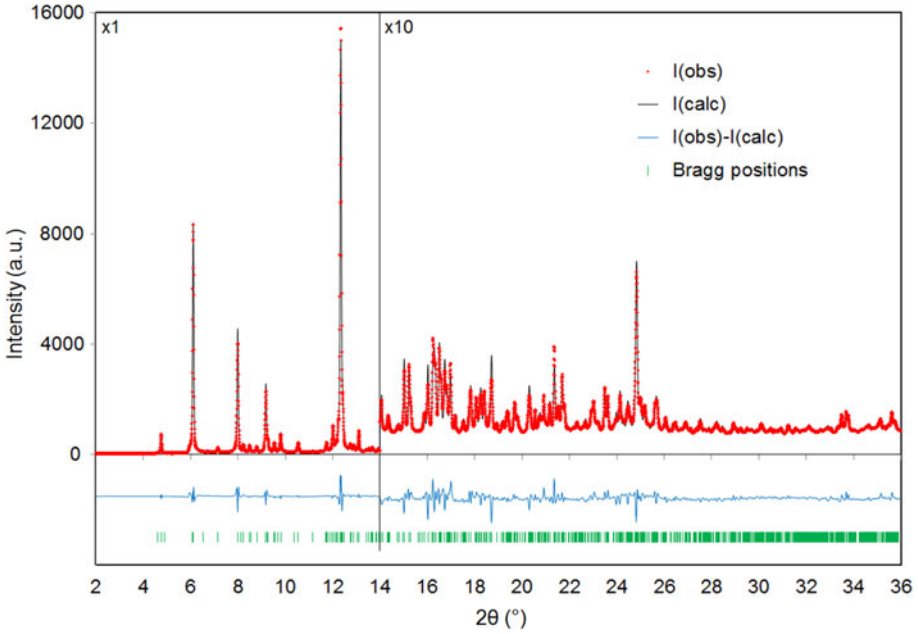

Figure 4. (color online) A plot of the final Rietveld refinement for hypoxanthine ($\chi^2 = 1.32$). The vertical scale has been multiplied by a factor of 10 for $2\theta > 14°$.

of the hypoxanthine sample with labeled chemical shifts and integral values. The two singlet peaks shown in Figure 5(a) at 7.97 and 8.11 ppm correspond to the expected shifts and splitting patterns of protons H_2 and H_8, respectively. The integral of the peak at 8.11 ppm was calibrated to a value of 1.00, which was used to calculate relative integral values of the other peaks. The peak at 7.97 ppm integrated to a value of 1.02, which is also consistent with the expected proton assignment. A comprehensive NMR study of hypoxanthine by Deng *et al.* (2004) indicates that the separation in chemical shift

TABLE II. The refined crystal structure of hypoxanthine ($\chi^2 = 1.32$, $R_p = 0.0624$, $R_{wp} = 0.0831$).

Atom	*x/a*	*y/b*	*z/c*	U_{iso} (Å^2)
Hypoxanthine molecule A				
N_{1A}	0.44677	0.71916	0.45912	0.0304 (7)
C_{2A}	0.45847	0.85732	0.45634	0.0304 (7)
N_{3A}	0.34148	0.99467	0.40074	0.0304 (7)
C_{4A}	0.20337	0.98466	0.34701	0.0304 (7)
C_{5A}	0.17971	0.85175	0.34350	0.0304 (7)
C_{6A}	0.31165	0.70481	0.40224	0.0304 (7)
O_{6A}	0.31497	0.57544	0.40480	0.0304 (7)
N_{7A}	0.02305	0.88878	0.27899	0.0304 (7)
C_{8A}	−0.04548	1.04201	0.24585	0.0304 (7)
N_{9A}	0.05695	1.10485	0.28394	0.0304 (7)
H_{1A}	0.53551	0.63993	0.49359	0.0397 (9)
H_{2A}	0.56121	0.85310	0.49696	0.0397 (9)
H_{8A}	−0.15988	1.10095	0.19658	0.0397 (9)
H_{9A}	0.04767	1.19646	0.28115	0.0397 (9)
Hypoxanthine molecule B				
N_{1B}	0.44089	0.34742	0.96653	0.0304 (7)
C_{2B}	0.44507	0.20476	0.96992	0.0304 (7)
N_{3B}	0.33010	0.18076	0.91492	0.0304 (7)
C_{4B}	0.19951	0.31557	0.85158	0.0304 (7)
C_{5B}	0.18382	0.46615	0.84035	0.0304 (7)
C_{6B}	0.31361	0.48937	0.89808	0.0304 (7)
O_{6B}	0.32505	0.61654	0.89335	0.0304 (7)
N_{7B}	0.03509	0.57244	0.76724	0.0304 (7)
C_{8B}	−0.03664	0.48783	0.73602	0.0304 (7)
N_{9B}	0.05878	0.33078	0.78466	0.0304 (7)
H_{1B}	0.53090	0.35234	1.01343	0.0397 (9)
H_{2B}	0.55258	0.12534	1.01693	0.0397 (9)
H_{8B}	−0.14875	0.52903	0.68019	0.0397 (9)
H_{9B}	0.04862	0.24611	0.76505	0.0397 (9)

The refined lattice parameters obtained are $a = 7.1179$ (2) Å, $b = 9.7830$ (3) Å, $c = 10.4009$ (3) Å, $\alpha = 58.876$ (1)°, $\beta = 67.609$ (1)°, and $\gamma = 71.937$ (2)°. All atom positions, in space group $P\bar{1}$ (#2), correspond to 2*i* Wyckoff sites with full occupancy.

https://doi.org/10.1017/S0885715615000457 Published online by Cambridge University Press

TABLE III. A comparison of the hydrogen bonding values for hypoxanthine from PXRD refinement and the single-crystal structure of Schmalle *et al.* (1988).

Bond D–H···A	PXRD D···A (Å)	Single crystal D···A (Å)
N_{1A}–H_{1A}···O_{6A}	2.787	2.779 (2)
N_{1B}–H_{1B}···O_{6B}	2.787	2.786 (3)
N_{9A}–H_{9A}···N_{7B}	2.815	2.802 (2)
N_{9B}–H_{9B}···N_{7A}	2.816	2.807 (3)
C_{8A}–H_{8A}···O_{6B}	3.207	3.146 (2)
C_{8B}–H_{8B}···O_{6A}	3.219	3.167 (4)
C_{2B}–H_{2B}···N_{3B}	3.357	3.348 (2)
C_{2A}–H_{2A}···N_{3A}	3.384	3.383 (4)

between these two aryl peaks is quite different for the N9H tautomer (0.01 ppm) and N7H tautomer (0.18 ppm). This has also been demonstrated using deuterated dimethylformamide as a solvent (Bartl *et al.*, 2009). Our observed separation of 0.14 ppm suggests that N7H tautomer is predominantly present in the DMSO solution and the N9H tautomeric form is negligible under the current experimental conditions. In contrast, the ratio of N7H and N9H tautomers was reported to be 58/42 (Chenon *et al.*, 1975), evaluated from the C4 and C5 chemical-shift Carbon-13 NMR data of hypoxanthine in DMSO at elevated temperature (37 and 58 °C). Deng *et al.*

TABLE IV. The reflection list obtained for hypoxanthine from the Rietveld refinement, including integrated intensities ≥ 0.3%, after summing reflections closer than 0.02° as multiple reflections and using a weighted average reflection position.

h	k	l	d_{obs} (Å)	$2\theta_{calc}$ (°)	$2\theta_{obs}$ (°)	I/I_{max} (%)	$\Delta 2\theta$ (°)
0	1	0	8.288 200	4.763	4.763	4.1	0.000
1	1	1	6.461 143	6.111	6.111	50.5	0.000
1	1	0	5.519 355	7.155	7.155	1.2	0.000
0	1	−1	4.942 110	7.992	7.992	28.8	0.000
0	1	2	4.796 518	8.235	8.235	1.4	0.000
0	2	1	4.647 787	8.499	8.499	1.4	0.000
1	2	1	4.492 165	8.794	8.794	1.0	0.000
1	−1	−1	4.304 126	9.179	9.179	15.6	0.000
0	0	2	4.285 027	9.220	9.220	0.7	0.000
1	2	2	4.258 756	9.277	9.277	2.1	0.000
0	2	0	4.144 210	9.534	9.534	1.5	0.000
1	0	2	4.130 810	9.565	9.565	0.8	0.000
0	2	2	4.029 527	9.806	9.806	4.3	0.000
1	2	0	3.747 497	10.546	10.546	2.2	0.000
2	1	2	3.365 215	11.748	11.748	2.0	0.000
1	−1	−2	3.301 100	11.977	11.977	0.9	0.000
1	−2	0	3.290 152	12.017	12.017	5.5	0.000
2	0	0	3.256 940	12.140	12.140	1.0	0.000
2	2	2	3.230 431	12.240	12.240	3.7	0.000
1	3	2	3.208 756	12.320	12.323	0.6	−0.003
0	2	−1	3.208 756	12.339	12.323	0.6	0.016
1	0	−2	3.203 318	12.344	12.344	100.0	0.000
0	1	3	3.181 751	12.428	12.428	7.9	0.000
1	−1	2	3.100 505	12.753	12.755	2.2	−0.002
0	2	3	3.100 505	12.761	12.755	2.2	0.006
0	3	1	3.067 220	12.894	12.894	1.5	0.000
0	3	2	3.031 404	13.047	13.047	0.4	0.000
2	0	2	3.016 671	13.111	13.111	4.8	0.000
1	−2	−2	2.946 425	13.425	13.425	0.6	0.000
1	3	3	2.921 945	13.538	13.538	1.0	0.000
2	−1	0	2.893 651	13.671	13.671	1.1	0.000
1	2	−1	2.885 878	13.708	13.708	0.4	0.000
2	1	3	2.837 878	13.941	13.941	0.9	0.000
2	−1	1	2.812 784	14.066	14.066	0.7	0.000
2	2	0	2.759 503	14.339	14.339	0.4	0.000
2	1	−1	2.634 709	15.022	15.022	1.7	0.000
1	2	4	2.599 443	15.228	15.227	1.8	0.001
2	3	1	2.587 450	15.298	15.298	0.5	0.000
1	1	4	2.494 443	15.872	15.872	0.5	0.000
0	2	−2	2.471 087	16.023	16.023	1.5	0.000
1	4	2	2.438 882	16.236	16.236	1.6	0.000
2	2	4	2.430 703	16.292	16.291	1.6	0.001
1	−3	0	2.422 138	16.349	16.349	1.2	0.000
2	−2	0	2.399 401	16.504	16.505	2.3	−0.001
0	2	4	2.399 401	16.514	16.505	2.3	0.009
1	−1	3	2.388 766	16.573	16.579	1.1	−0.006
1	4	3	2.388 766	16.586	16.579	1.1	0.007
1	−2	2	2.366 795	16.734	16.734	1.8	0.000
2	3	4	2.354 641	16.821	16.821	1.0	0.000
3	2	2	2.333 434	16.975	16.975	1.7	0.000
1	4	1	2.305 795	17.180	17.180	0.3	0.000

Continued

https://doi.org/10.1017/S0885715615000457 Published online by Cambridge University Press

TABLE IV. Continued

h	k	l	d_{obs} (Å)	$2\theta_{calc}$ (°)	$2\theta_{obs}$ (°)	I/I_{max} (%)	$\Delta 2\theta$ (°)
1	3	−1	2.234 188	17.735	17.735	0.3	0.000
0	4	3	2.222 380	17.816	17.830	1.4	−0.014
1	0	4	2.222 380	17.834	17.830	1.4	0.004
1	−3	−3	2.195 513	18.038	18.050	0.6	−0.012
3	1	3	2.195 513	18.056	18.050	0.6	0.006
3	0	2	2.191 059	18.087	18.087	0.4	0.000
3	1	0	2.178 043	18.196	18.196	0.3	0.000
3	0	0	2.171 181	18.254	18.254	1.0	0.000
3	3	2	2.156 656	18.378	18.378	0.4	0.000
3	3	3	2.152 244	18.405	18.416	0.9	−0.011
2	−2	−2	2.152 244	18.417	18.416	0.9	0.001
2	−1	3	2.122 429	18.677	18.677	0.4	0.000
1	1	−3	2.118 494	18.712	18.712	1.6	0.000
2	0	4	2.065 455	19.197	19.197	0.3	0.000
3	2	0	2.047 391	19.368	19.368	0.4	0.000
0	4	4	2.014 737	19.685	19.685	0.5	0.000
1	−2	−4	2.012 510	19.707	19.707	0.4	0.000
2	−1	−3	1.953 739	20.304	20.306	1.1	−0.002
0	3	−2	1.953 739	20.311	20.306	1.1	0.005
1	5	2	1.930 694	20.552	20.551	0.5	0.001
2	−3	−2	1.911 193	20.761	20.763	0.4	−0.002
1	−3	−4	1.911 193	20.767	20.763	0.4	0.004
2	1	5	1.897 187	20.910	20.918	0.8	−0.008
2	5	3	1.897 187	20.919	20.918	0.8	0.001
1	5	4	1.874 419	21.171	21.175	0.7	−0.004
2	4	0	1.874 419	21.182	21.175	0.7	0.007
2	−3	1	1.858 285	21.360	21.361	2.0	−0.001
2	5	4	1.858 285	21.372	21.361	2.0	0.011
2	5	2	1.847 175	21.491	21.491	0.4	0.000
0	5	3	1.841 671	21.556	21.556	0.5	0.000
3	3	5	1.830 178	21.693	21.693	1.4	0.000
1	5	1	1.822 624	21.784	21.784	0.6	0.000
1	5	5	1.731 693	22.943	22.943	0.5	0.000
4	3	3	1.726 275	23.016	23.016	0.8	0.000
3	−2	2	1.691 702	23.492	23.493	1.1	−0.001
1	2	6	1.691 702	23.505	23.493	1.1	0.012
4	2	4	1.682 664	23.622	23.621	0.9	0.001
3	−2	−2	1.657 970	23.978	23.978	0.4	0.000
2	−1	−4	1.657 970	23.981	23.978	0.4	0.003
1	−1	−5	1.647 276	24.135	24.136	1.2	−0.001
2	4	−1	1.647 276	24.149	24.136	1.2	0.013
0	2	−4	1.625 062	24.457	24.471	0.9	−0.014
1	−3	3	1.625 062	24.475	24.471	0.9	0.004
1	6	4	1.604 918	24.783	24.783	0.5	0.000
2	0	−4	1.601 610	24.835	24.835	5.1	0.000
4	2	0	1.595 225	24.936	24.936	0.3	0.000
0	2	6	1.590 768	25.004	25.007	0.9	−0.003
3	−3	−1	1.590 768	25.009	25.007	0.9	0.002
4	−1	1	1.580 013	25.174	25.180	0.8	−0.006
3	2	6	1.580 013	25.181	25.180	0.8	0.001
1	−5	0	1.554 274	25.604	25.604	0.3	0.000
2	−2	4	1.550 464	25.668	25.668	0.7	0.000
2	6	2	1.548 388	25.702	25.703	0.4	−0.001
3	5	1	1.548 388	25.706	25.703	0.4	0.003
2	3	7	1.480 188	26.909	26.909	0.3	0.000
5	5	5	1.291 664	30.916	30.928	0.3	−0.012
2	1	−5	1.291 664	30.934	30.928	0.3	0.006
2	5	8	1.279 599	31.214	31.227	0.3	−0.013
5	1	5	1.279 599	31.233	31.227	0.3	0.006
5	1	6	1.195 678	33.479	33.481	0.3	−0.002
1	8	3	1.195 678	33.484	33.481	0.3	0.003
1	−7	−1	1.188 644	33.685	33.685	0.4	0.000
4	7	7	1.185 671	33.772	33.772	0.4	0.000
5	7	5	1.141 389	35.124	35.124	0.4	0.000
1	−6	2	1.141 389	35.125	35.124	0.4	0.001
5	0	6	1.126 551	35.602	35.602	0.5	0.000
2	−7	−3	1.122 069	35.749	35.749	0.3	0.000

https://doi.org/10.1017/S0885715615000457 Published online by Cambridge University Press

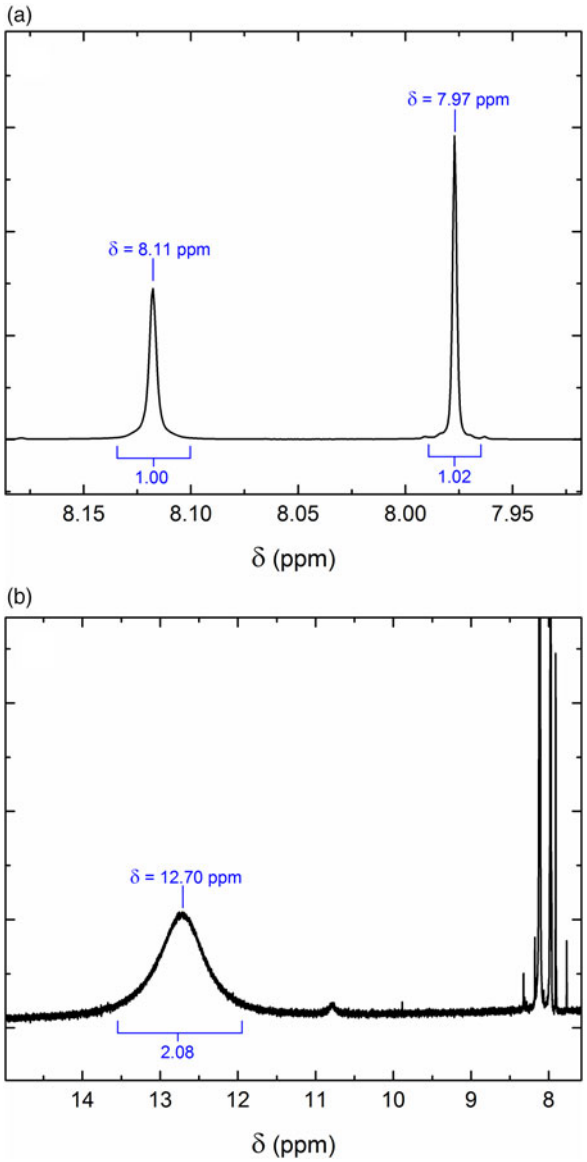

Figure 5. (color online) The ^{1}H-NMR spectrum observed for the hypoxanthine sample for chemical shifts between (a) a narrow range of 7.92 and 8.18 ppm and (b) a wide range of 7.5–15 ppm.

(2004) obtained a similar ratio (55/45), evaluated from the intensity ratio of N7H and N9H peaks in the proton NMR spectrum of hypoxanthine in a mixture of 55% DMSO and 45% acetonitrile at low temperature (−40 °C). It is noted that the two aryl peaks of hypoxanthine appear at 8.17 and 8.20 ppm in aqueous solution, suggesting that the N9H tautomer is predominantly present in water.

Figure 5(b) shows a very broad peak found at 12.70 ppm, with a relative integral value of 2.08 (integrated from 12.0 to 13.6 ppm), which is characteristic of a highly de-shielded amine. It is interesting to note that a broad peak was also observed at 12.8 ppm in the proton NMR spectrum of 4 (3H)-pyrimidinone in DMSO, which corresponds to the chemical shift of H_1 (Saladino *et al.*, 2001). Our *ab initio* calculations predicted that the chemical shifts of H_1, H_7, and H_9 in the keto form should be very similar, whereas that of H_6 from the enol form would be located further upfield by 2–3 ppm (see Tables V–VII). The experimental chemical shifts of the H_9, H_7, and H_1 protons tabulated by Deng *et al.* (2004) for the keto form of hypoxanthine fall between 12.4 and 13.7 ppm, which are consistent with the location of the broad peak observed in this work. The differences between the calculated and observed chemical shifts are because of the strong hydrogen bonding in DMSO, which is not accounted for in the *ab initio* calculations. As N9H is negligible, an integral of 2 indicates that the broad peak in our NMR spectrum can be attributed to H_1 and H_7 (each with an integral of 1), which further suggests that hypoxanthine is predominantly in its keto form in DMSO at room temperature. The small peak at 10.77 ppm with an integral value of 0.12 may be attributed to H_6, which suggests a minor presence of the enol form of hypoxanthine under these conditions.

TABLE V. The calculated ^{1}H chemical shifts of the keto N9H tautomer of hypoxanthine in DMSO.

Nuclei	Atom	δ_{calc} (ppm) (this work)	δ_{calc} (ppm) (Deng *et al.*, 2004)
^{1}H	N–1H	7.88	7.54
	C–2H	7.76	7.71
	C–8H	7.65	7.50
	N–9H	8.31	8.11

TABLE VI. The calculated ^{1}H chemical shifts of the keto N7H tautomer of hypoxanthine in DMSO.

Nuclei	Atom	δ_{calc} (ppm) (this work)	δ_{calc} (ppm) (Deng *et al.*, 2004)
^{1}H	N–1H	7.85	7.53
	C–2H	7.91	7.86
	C–8H	7.86	7.72
	N–7H	8.72	8.56

TABLE VII. The calculated ^{1}H chemical shifts of the enol N9H tautomer of hypoxanthine in DMSO.

Nuclei	Atom	δ_{calc} (ppm) (this work)
^{1}H	O–H	5.79
	N–9H	6.37
	C–2H	8.58
	C–8H	7.84

ACKNOWLEDGEMENTS

The authors thank the Saskatchewan Structural Sciences Centre (SSSC) for access and assistance with the collection of the NMR data. Research described in this paper was performed using beamlines 08B1-1 and 11ID-1 at the Canadian Light Source, which is supported by the Canadian Foundation for Innovation, the Natural Sciences and Engineering Research Council of Canada, the National Research Council of Canada, the Canadian Institutes of Health Research, the Government of Saskatchewan, Western Economic Diversification Canada, and the University of Saskatchewan.

Allen, F. H. (**2002**). "The Cambridge structural database: a quarter of a million crystal structures and rising," Acta Crystallogr. B **58**, 380–388.

Bartl, T., Zacharová, Z., Sečkářová, P., Kolehmainen, E. and Marek, R. (**2009**). "NMR quantification of tautomeric populations in biogenic purine bases," Eur. J. Org. Chem. **9**, 1377–1383.

https://doi.org/10.1017/S0885715615000457 Published online by Cambridge University Press

Batey, R. T., Gilbert, S. D. and Montange, R. K. (**2004**). "Structure of a natural guanine-responsive riboswitch complexed with the metabolite hypoxanthine," Nature **432**, 411–415.

Becke, A. D. (**1988**). "Density-functional exchange-energy approximation with correct asymptotic behavior," Phys. Rev. A **38**(6), 3098–3100.

Chenon, M. T., Pugmire, R. J., Grant, D. M., Panzica, R. P. and Townsend, L. B. (**1975**). "Carbon-13 magnetic resonance. XXVI. Quantitative determination of the tautomeric populations of certain purines," J. Am. Chem. Soc. **97**, 4636–4642.

Deng, H., Cahill, S. M., Abad, J. L., Lewandowicz, A., Callender, R. H., Schramm, V. and Jones, R. A. (**2004**). "Active site contacts in the purine nucleoside phosphorylase-hypoxanthine complex by NMR and *ab initio* calculations," Biochemistry **43**, 15966–15974.

Dinnebier, R. E. (**1999**). "Rigid bodies in powder diffraction: a practical guide," Powder Diffr. **14**, 84–92.

Gallant, B. M., Mitchell, R. R., Kwabi, D. G., Zhou, J., Zuin, L., Thompson, C. V. and Shao-Horn, Y. (**2012**). "Chemical and morphological changes of Li–O_2 battery electrodes upon cycling," J. Phys. Chem. C **116**, 20800–20805.

ICDD (**2013**), *PDF-4+ 2013 (Database)* edited by Dr. Soorya Kabekkodu (International Centre for Diffraction Data, Newtown Square, PA, USA).

Krylov, A. I. and Gill, P. M. W. (**2013**). "Q-Chem: an engine for innovation," WIREs Comput. Mol. Sci. **3**, 317–326.

Lake, C. H. and Toby, B. H. (**2011**). "Rigid body refinements in GSAS/EXPGUI," Powder Diffr. **26**, S13–S21.

Larson, A. C. and Von Dreele, R. B. (**2004**). *General Structure Analysis System (GSAS)* (Report No. LAUR 86-748), Los Alamos, NM: Los Alamos National Laboratory.

Lee, C., Yang, W. and Parr, R. G. (**1988**). "Development of the Colle-Salvetti correlation-energy formula into a functional of the electron density," Phys. Rev. B **37**(2), 785–789.

Marat, K. (2014). Spinworks: NMR Processing Software (Version 4.0.5.0). Available from http://home.cc.umanitoba.ca/~wolowiec/spinworks/

Pang, B., McFaline, J. L., Burgis, N. E., Dong, M., Taghizadeh, K., Sullivan, M. R., Elmquist, C. E., Cunningham, R. P. and Dedon, P. C. (**2012**). "Defects in purine nucleotide metabolism lead to substantial incorporation of xanthine and hypoxanthine into DNA and RNA," Proc. Nat. Acad. Sci. USA **109**, 2319–2324.

Parker, R., Snedden, W. and Watts, R. W. E. (**1969**). "The mass-spectrometric identification of hypoxanthine and xanthine ('oxypurine') in skeletal muscle from two patients with congenital xanthine oxidase deficiency (xanthinuria)," Biochem. J. **115**, 103–108.

Puig, J. G., Mateos, F. A., Jimenez, M. L. and Ramos, T. H. (**1988**). "Renal excretion of hypoxanthine and xanthine in primary gout," Am. J. Med. **85**, 533–537.

Reid, J. W., Kaduk, J. A., Garimella, S. V. and Tse, J. S. (**2015**). "Rietveld Refinement using synchrotron powder diffraction data for curcumin, $C_{21}H_{20}O_6$, and comparison with density functional theory," Powder Diffr. **30**, 67–75.

Saladino, R., Crestini, C., Costanzo, G., Negri, R., and Di Mauro, E. (**2001**). "A possible prebiotic synthesis of purine, adenine, cytosine, and 4 (3H)-pyrimidinone from formamide: implications for the origin of life," Bioorg. Med. Chem. **9**, 1249–1253.

Samuel, N. T., Lee, C. Y., Gamble, L. J., Fischer, D. A. and Castner, D. G. (**2006**). "NEXAFS characterization of DNA components and molecular-orientation of surface-bound DNA oligomers," J. Electron Spectrosc. Rel. Phenom. **152**, 134–142.

Sarkar, S. D. and Nahar, L. (**2007**). *Chemistry for Pharmacy Students* (Wiley, New York).

Schmalle, H. W., Hänggi, G. and Dubler, E. (**1988**). "Structure of hypoxanthine," Acta Crystallogr. C **44**, 732–736.

Toby, B. H. (**2001**). "EXPGUI, a graphical user interface for GSAS," J. Appl. Crystallogr. **34**, 210–213.

Toby, B. H. and Von Dreele, R. B. (**2013**). "GSAS II: the genesis of a modern open-source all-purpose crystallography software package," J. Appl. Crystallogr. **46**, 544–549.

Yang, R. Q. and Xie, Y. R. (**2007**). "A monoclinic polymorph of hypoxanthine," Acta Crystallogr. E **63**, o3309.

Zhou, J., Hu, Y., Li, X., Wang, C. and Zuin, L. (**2014**). "Chemical bonding in amorphous Si-coated carbon nanotubes as anodes for Li ion batteries: a XANES study," RSC Adv. **4**, 20226–20229.

Zubavichus, Y., Shaporenko, A., Korolkov, V., Grunze, M. and Zharnikov, M. (**2008**). "X-ray absorption spectroscopy of the nucleotide bases at the carbon, nitrogen, and oxygen K-edges," J. Phys. Chem. B **112**, 13711–13716.

https://doi.org/10.1017/S0885715615000457 Published online by Cambridge University Press